Production of Si by Vacuum Carbothermal Reduction of SiO_2 using Concentrated Solar Energy

Peter G. Loutzenhiser, Ozan Tuerk, and Aldo Steinfeld

Using concentrated solar radiation as the energy source of high-temperature process heat, the carbothermal reduction of silica to silicon was examined thermodynamically and demonstrated experimentally at vacuum pressures. Reducing the system pressure favors Si(g) formation, enabling its vacuum distillation. Experimentation in a solar reactor was performed in the range 1,997–2,263 K at ~3×10^{-3} bar with mixtures of charcoal and silica directly exposed to radiative flux intensities equivalent to 6,500 suns, yielding Si purities ranging from 66.1–79.2 wt.%. The Si purity increased with temperature. Solid characterizations showed SiC and SiO as important reaction intermediaries.

INTRODUCTION

Silicon is a valuable metalloid and a primary component for manufacturing electronic semiconductors and photovoltaic (PV) cells. However, silicon is rarely found free in nature and must be extracted by reducing readily available silica via a highly energy-intensive process. Conventional production methods use electric arc furnaces and require about 2.9 tons of quartz sand, 1.9 tons of coke, 0.12 tons of graphite (electrodes), and 12.5 MWh electricity per ton of metallurgical-grade silicon (MGS) produced,[1,2] while releasing at least 17 tons of CO_2 when using coal-fired electricity. Alternatively, concentrated solar energy can be used as a high-temperature heat source to drive the endothermic reduction and, thus, avoid concomitant greenhouse gas emissions derived from fossil-fuel-based processes. When the reducing agent is biomass charcoal, the solar-driven carbothermal reduction is CO_2 neutral. An additional energy-intensive refining step is required for obtaining high-purity Si employed in electronic and PV applications.[3–5] The purification of MGS by extraction of B and P was experimentally demonstrated using concentrated solar energy in the temperature range 1,823–1,975 K.[6]

Early exploratory work on the carbothermal reduction of SiO_2 using a solar furnace yielded α-Si_3N_4 and SiC as the main solid products when the solar reactor was operated at 1,773 K in an N_2 atmosphere at 1 bar.[7] Consequently, a two-step process was proposed involving the production of Si_3N_4 followed by its dissociation to its elements at above 1,800 K.[8] The reaction kinetics of the first step was determined in a tube furnace.[9] Other carbothermal reductions for metal extraction from oxides using concentrated solar energy were experimentally investigated for Fe_2O_3,[10] ZnO,[11–13] MgO,[14] and Al_2O_3.[15] A further step to make the reaction thermodynamically favorable and avoid undesired byproducts (e.g., carbides) consists of decreasing the total pressure, which lowers the onset temperature of metal vapor formation and enables its vacuum distillation. This was recently demonstrated for the carbothermal reduction of Al_2O_3 to Al.[16] In the present study, a thermodynamic analysis was performed over the range 1,000–3,000 K at 10^{-6}, 10^{-3}, and 1 bar to determine equilibrium compositions and identify experimental operating conditions. Experimentation was carried out with a solar reactor operated at ~3×10^{-3} bar and exposed to simulated high-flux solar radiation. The aim of these experiments was to examine the process feasibility, ascertain overall chemical conversions and purities as a function of temperatures and molar ratios, and identify the reaction scheme. (See the sidebar for nomenclature definitions.)

How would you…

…describe the overall significance of this paper?

It has been thermodynamically shown and experimentally demonstrated that it is possible to reduce silica and distill silicon vapor under vacuum conditions using highly concentrated solar radiation as the energy source of high-temperature process heat. When the reducing agent is biomass charcoal, the solar-driven carbothermal process is CO_2 neutral.

…describe this work to a materials science and engineering professional with no experience in your technical specialty?

Concentrated solar energy delivers heat at temperatures above 2,000 K and enables the highly endothermic reaction of silica and bio-charcoal. The solar-driven production of silicon eliminates concomitant emissions derived from conventional processes.

…describe this work to a layperson?

A novel solar thermochemical process is reported to produce silicon—widely used in electronics and photovoltaics—from readily available silica using concentrated sunlight and a carbon-containing reducing agent. Theoretical and experimental analyses showed this can be accomplished by creating a vacuum in the solar reactor and distilling silicon vapor. The solar-based process is more environmentally friendly than conventional fossil-fuel-based processes.

THERMODYNAMIC ANALYSIS

Equilibrium composition computations were performed using the software code HSC.[17] Species with mole fractions of less than 10^{-5} were omitted from the figures. The thermal dissociation of

SiO_2 at 1 bar is favorable at above 3,300 K, forming SiO(g) and above 4,200 K, Si(g). The reduction temperature can be significantly decreased via a carbothermal reduction, represented stoichiometrically as Equation 1 (all equations are in the table on page 52).

The variation of the equilibrium composition of the system SiO_2+2C with temperature at 1 bar is shown in Figure 1. The reaction proceeds at above 1,700 K to form SiC along with small amounts of gaseous SiO(g) and CO(g). At above 2,000 K, SiO_2 and C are no longer stable at equilibrium. The formation of SiO(g) and CO(g) increases with temperature and is coupled to decreasing SiC, but the equilibrium amounts remain constant over the range 2,100–2,500 K. Above 2,500 K, both Si(g) and Si are predicted in increasing amounts.

The effect of the total system pressure was examined on the chemical conversion, defined as Equation 2, where n^{eq} and n^{in} are the equilibrium and initial molar amounts, respectively, of a given species j = SiO_2, Si(g), SiC, and SiO(g). The analysis was performed at 10^{-6}, 10^{-3}, and 1 bar. Figure 2a shows X_{SiO_2} and $X_{Si(g)}$ and Figure 2b shows X_{SiC} and $X_{SiO(g)}$ as functions of T^{eq} and p. Consistent with the Le Chatelier's principle, lowering the total pressure of the system results in a shift of the equilibrium to the more favorable formation of Si(g) at lower temperatures. X_{SiC} and X_{SiO} are also shifted to lower T^{eq} for lower p. At $p = 10^{-6}$ bar, SiC and SiO(g) are the dominant products over the range 1,400–2,000 K, and rapidly decrease as Si(g) becomes more thermodynamically favorable. Thus, operating at vacuum pressures avoids undesired by-products SiC and SiO(g) while enabling the vacuum distillation of Si(g).

See the sidebar for experimental details.

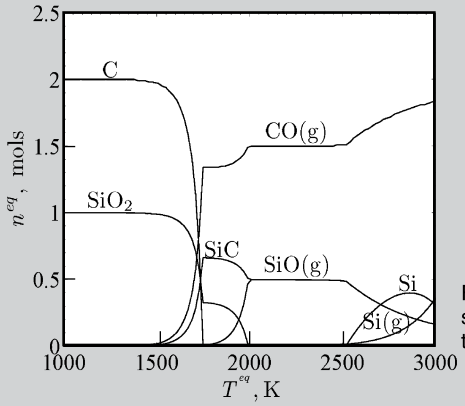

Figure 1. Equilibrium compositions of the system SiO_2+2C as a function of temperature at 1 bar.

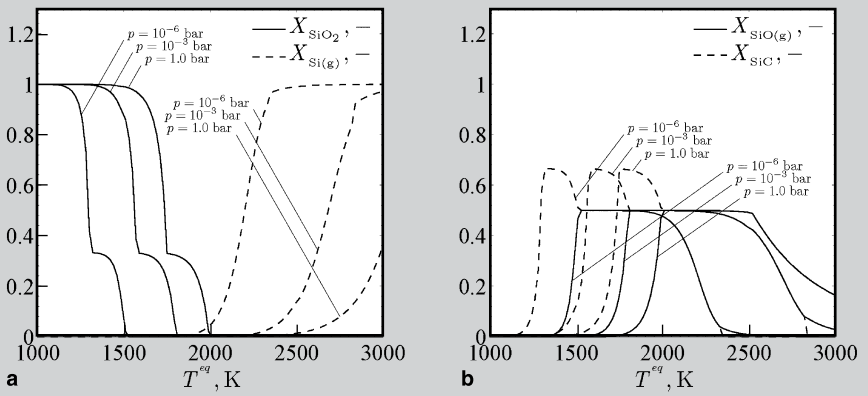

Figure 2. Chemical conversions versus equilibrium temperature at 10^{-6}, 10^{-3}, and 1 bar for: (a) SiO_2 (solid) and Si(g) (dashed); and (b) SiO(g) (solid) and SiC(dashed).

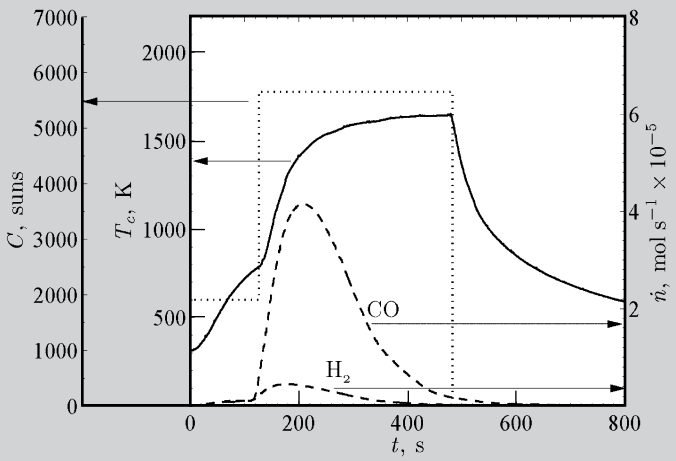

Figure 3. Molar flow rates of CO and H_2 (dashed), backside crucible temperature (solid), and solar concentration ratio (dotted) measurements as a function of time during a representative solar experimental run with a C: SiO_2 molar ratio of 2.

NOMENCLATURE

A	=	absorptance
C	=	solar concentration ratio
d	=	crucible thickness
E_b	=	Planck's total blackbody emissive power
F	=	configuration factor
f	=	fractional function
h	=	convective heat transfer coefficient
H_o	=	external contribution to irradiation
k	=	thermal conductivity
m	=	mass
M	=	molecular weight
n	=	molar amount
N	=	total number of surfaces
p	=	pressure
q	=	net radiative flux
R	=	reflectance
r_m	=	mass ratio of product in the crucible after experimentation to the initial reactants
T	=	temperature
V	=	transmittance
X	=	chemical conversion

Greek Symbols

α	=	purity
$\bar{\alpha}$	=	molar purity
$\Delta H^{\circ}_{298.15K}$	=	standard enthalpy change
Δt	=	time increment
ε	=	emissivity
λ_c	=	cutoff wavelength
σ	=	Stefan-Boltzmann constant

Superscripts

eq	=	equilibrium condition
in	=	initial condition

Subscripts

amb	=	ambient conditions
c	=	crucible
g	=	guess
surface	=	crucible surface

RESULTS AND DISCUSSION

A total of 14 experimental runs was carried out for varying $n_C^{in}/n_{SiO_2}^{in}$ and temperature by adjusting C in the range 5,362–6,748 suns. A representative run is shown in Figure 3 for stoichiometric $n_C^{in}/n_{SiO_2}^{in} = 2$. The reactants were initially exposed to a solar radiative flux equivalent to C = 1,910 suns during 120 s to affect the release of volatiles contained in the charcoal by pyrolysis. This was coupled to a rapid increase in T_c to ~800 K with formation of small amounts of CO and H_2 detected in outlet gas flow. C was then increased to 5,660 suns, resulting in a rise of T_c to 1,400 K over 50 s. Relatively large amounts of CO, evidence of the carbothermal reduction, were measured along with H_2—indicative of the incomplete pyrolysis of charcoal. T_c began to stabilize after 200 s and the CO gas evolution decreased as the reaction neared completion.

EXPERIMENTAL SETUP

Experimentation was carried out at PSI's High-Flux Solar Simulator (HFSS):[18] an array of ten 15 kW_e high-pressure Xenon arcs, each closed-coupled with truncated ellipsoidal specular reflectors of common focus. This unique facility provides an external source of intense thermal radiation, mostly in the visible and infrared (IR) spectra, that closely approximates the heat transfer characteristics of highly concentrating solar systems such as solar towers and solar parabolic dishes. Power flux intensities are adjustable by the number of Xe arcs in operation, the position of the venetian-blind shutter, and the position of the test target relative to the focal plane. Radiative fluxes incident into the reactor were measured optically with a calibrated charge-coupled device (CCD) camera on a water-cooled Al_2O_3-plasma coated Lambertian target. The reactants were directly exposed to peak solar concentration ratios C exceeding 6,500 suns. (The solar concentration ratio C is defined as the solar radiative flux normalized to 1 kW/m^2. C is often expressed in units of "suns.")

The solar reactor is shown schematically in Figure A. It consists of a transparent quartz tube (length 150 mm, diameter 40 mm, wall thickness 2 mm) containing a glassy carbon crucible (Sigradur G, diameter 29 mm, height 15 mm, thickness 2 mm) supported by a ZrO_2/Al_2O_3 holder and loaded with solid reactants. A type-S thermocouple in contact with the backside of the crucible was used to temporally monitor temperature T_c during experimentation. The reactor was vertically positioned while a water-cooled 45°-mirror redirected the incoming concentrated radiation towards the crucible ("beam-down" optics). The quartz tube was closed at the top and had a side inlet for Ar flow, which served as a carrier for emerging gaseous species. The bottom of the quartz tube was mounted on a water-cooled steel plate and kept sealed tight with Viton O-rings protected from spilled radiation by an Al_2O_3 shield. The gas outlet at the bottom was connected to a water-cooled condenser, a paper filter (Whatman, Grade GF/A: 1.6 µm), and a vacuum pump (Alcatel 20012A, dual stage, rotary vane, maximal flow 12 m^3/h). The vacuum pump was used to evacuate the reactor to a total pressure of ~3×10^{-3} bars, measured with a vacuum differential pressure sensor (SMC PSE-540). The Ar mass flow rate was maintained at 0.5 l_N min^{-1} (l_N means liters under normal conditions at 273.15 K and 1 atm.), controlled with an electronic flowmeter (Bronkhorst HI-TEC). Product gas composition was monitored on-line by an IR gas analyzer (Ultramat 23, 0.2% detection limit, 1 s^{-1} sampling rate). Composition of solid products was determined by x-ray powder diffraction (XRD, Philips XPert MPD/DY636, CuK_α, λ= 1.540598 Å, 2θ=20–80°, step size 0.05°) and inductively coupled plasma-optical emission spectrometry (ICP, Varian; Vista XX). Solid samples were characterized by means of their particle size distribution measured by laser scattering (HORIBA LA-950 analyzer), BET specific surface area measured by N_2 adsorption at 77 K (Micromeritics TriStar 3000), and morphologies by scanning electron microscopy (SEM SmartSEM, Carl Zeiss Supra 55VP).

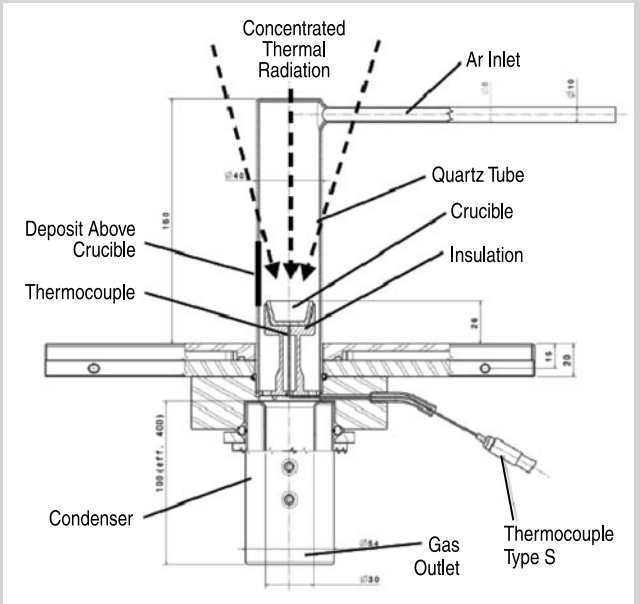

Figure A. Schematic of the solar reactor.

High purity silica (Sigma-Aldrich S5631) was mixed with biocharcoal (FLUKA 03866, powdered retort beech-charcoal, carbon content 81%) in C:SiO_2 molar ratios $n_C^{in}/n_{SiO_2}^{in}$ = 1, 2, and 4. The particle size distributions for both reactants are given in Figure B. For silica, it was a log-normal distribution with Sauter mean particle size of 2.4 µm. For charcoal, it was a bimodal distribution with Sauter mean particle size of 38.2 µm. BET specific surface areas were 8.11 and 65.6 m^2/g for silica and charcoal, respectively. An initial mass of the mixture of ~0.5 g was loaded for all experiments.

Pyrometric measurement of the surface temperatures was not possible because of the reflected incident radiation. Surface temperatures of the exposed reactants were calculated by applying a heat transfer model (described in sidebar on page 53).

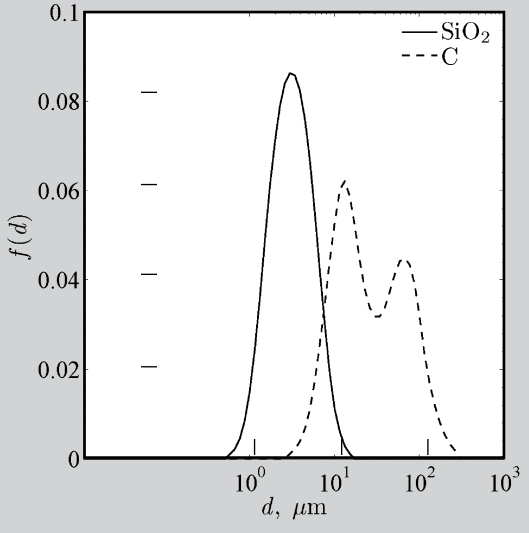

Figure B. Particle-size distributions for silica (solid curve) and charcoal (dashed curve).

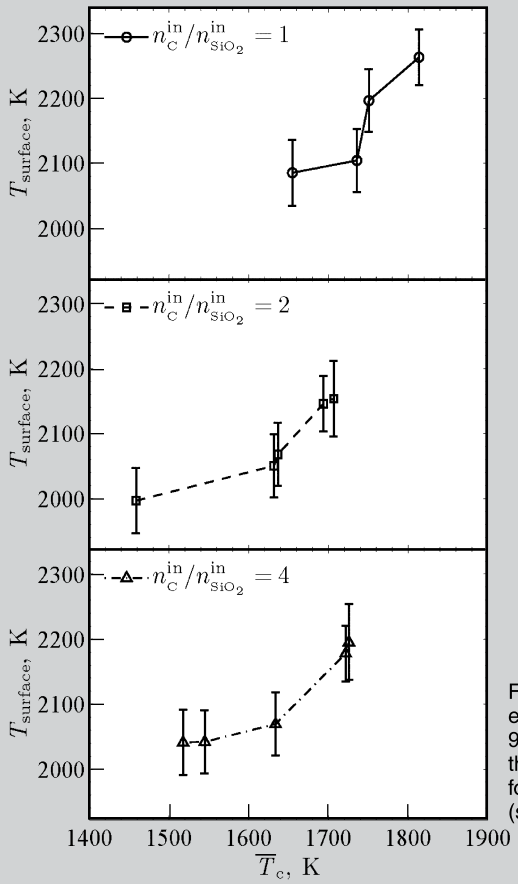

Figure 4. Surface temperature of exposed reactants, calculated with 95% error bounds, as a function of the backside crucible temperature for C:SiO_2 molar ratio of 1 (circles), 2 (squares), and 4 (triangles).

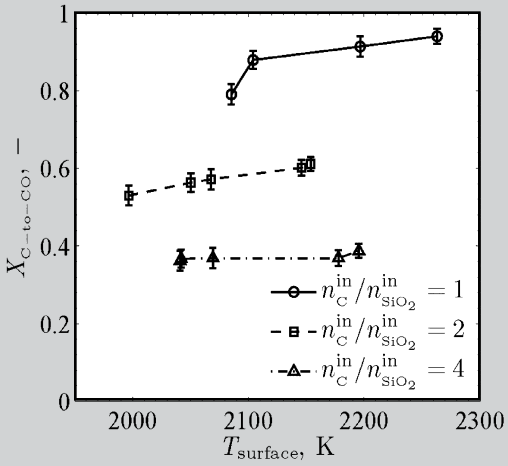

Figure 5. Chemical conversions from C to CO, with 95% error bounds, as a function of the surface temperature for C:SiO_2 molar ratio of 1(circles), 2 (squares), and 4 (triangles). Ninety-five percent error bounds computed from propagation error analysis are indicated in the data points.

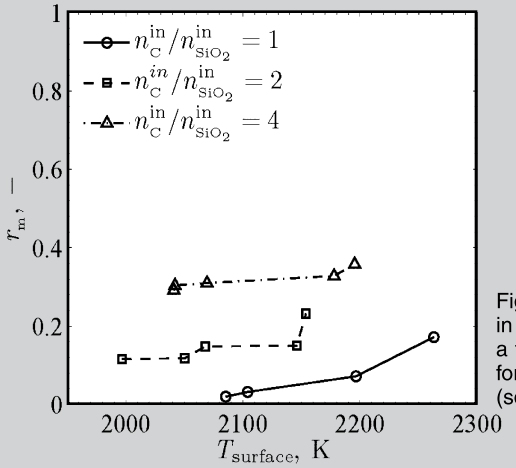

Figure 6. Mass ratio of solid products in the crucible to the initial reactants as a function of the surface temperature for C:SiO_2 molar ratio of 1(circles), 2 (squares), and 4 (triangles).

After 480 s, the HFSS was turned off and very little gas evolution was detected as the system cooled and T_c rapidly decreased. Semi-transparent black/brown depositions on the quartz tube (~2 cm above the crucible) were observed after each experiment, but these did not obstruct the incoming concentrated thermal radiation.

Surface Temperature

The heat transfer model (see sidebar on page 53) was applied using measured C and $\overline{T}_c$ – averaged over the final 40 s of radiative exposure – as inputs. $T_{surface}$, calculated with 95% error bounds, is provided in Figure 4 as a function of $\overline{T}_c$ for $n_C^{in}/n_{SiO_2}^{in}$ = 1, 2, and 4. The large error bounds are evidence of large uncertainties of the input parameters propagating through the model predictions. Overall, the predicted $T_{surface}$ ranged from 2,027 to 2,291 K; the lowest obtained for $n_C^{in}/n_{SiO_2}^{in}$ = 2 and the highest for $n_C^{in}/n_{SiO_2}^{in}$ = 1. See the sidebar for surface temperature details.

Chemical Conversion

The chemical conversion of C to CO was calculated as Equation 3, where $\dot{n}_{CO}$ is the molar flow rate of CO computed assuming ideal gas behavior, Δt is the time increment between sampling, and n_C^{in} is the initial molar amount of C in charcoal. $X_{C\text{-to-}CO}$ is shown in Figure 5 as a function of the $T_{surface}$ for $n_C^{in}/n_{SiO_2}^{in}$

Equations

$$SiO_2 + 2C \rightarrow Si + 2CO \qquad \Delta H^{\circ}_{298.15K} = 689.8 \text{ kJ mol}^{-1} \tag{1}$$

$$X_j = \frac{n_j^{eq}}{n_{SiO_2}^{in}} \tag{2}$$

$$X_{C\text{-to-}CO} = \frac{\sum \dot{n}_{CO} \Delta t}{n_C^{in}} \tag{3}$$

$$\overline{\alpha}_{Si} = \frac{\alpha_{Si}/M_{Si}}{\alpha_{Si}/M_{Si} + (1-\alpha_{Si})/M_{SiO_2}} \tag{4}$$

$$SiO_2 + 3C \rightarrow SiC + 2CO \tag{5}$$

$$2SiO_2 + SiC \rightarrow 3SiO + CO \tag{6}$$

$$SiO + 2C \rightarrow SiC + CO \tag{7}$$

$$SiO + SiC \rightarrow 2Si + CO \tag{8}$$

= 1, 2, and 4. Ninety-five percent error bounds computed from propagation error analysis are indicated in the data points. The lowest $X_{\text{C-to-CO}}$ of just below 0.4 occurred when $n_{\text{C}}^{\text{in}}/n_{\text{SiO}_2}^{\text{in}} = 4$ with excess charcoal, while the highest $X_{\text{C-to-CO}}$ of 0.8–0.95 occurred at $n_{\text{C}}^{\text{in}}/n_{\text{SiO}_2}^{\text{in}} = 1$ with deficiency of charcoal. $X_{\text{C-to-CO}}$ increased with T_{surface} for all three $n_{\text{C}}^{\text{in}}/n_{\text{SiO}_2}^{\text{in}}$.

Solid Characterization

Figure 6 shows the mass ratio of solid products in the crucible to the initial solid reactants, r_{m}, as a function of T_{surface} for all experiments. As expected, the highest r_{m} was for $n_{\text{C}}^{\text{in}}/n_{\text{SiO}_2}^{\text{in}} = 4$ with excess charcoal and the lowest r_{m} was for $n_{\text{C}}^{\text{in}}/n_{\text{SiO}_2}^{\text{in}} = 1$ with deficiency of charcoal. r_{m} increased with T_{surface} for all $n_{\text{C}}^{\text{in}}/n_{\text{SiO}_2}^{\text{in}}$ as sintering and melting of reacting solids hindered the distillation.

X-ray diffraction analyses of crucible products detected SiC and, for some cases, Si in the system, consistent with thermodynamic equilibrium calculations (Figure 2). XRD analysis of samples scraped from the quartz tube after experimentation detected pure Si in all but three cases where SiO_2 was also detected. Formation of amorphous SiO(s) was possible due to vacuum pressures and rapid cooling on the inner surface of the much cooler quartz tube.[23] Presumably, metastable SiO(s) disproportionated to a more stable mixture of Si and SiO_2 upon cooling. SEM pictures of reactants and product samples collected from the crucible and scraped from the quartz tube are shown in Figure 7 a, b, and c, respectively.

ICP analysis was used to determine the Si purity of samples collected from the quartz tube. The molar purity of Si in Si-SiO_2 mixtures was calculated as Equation 4, where α_{Si} is silicon purity and M is the molecular weight. Figure 8 shows α_{Si} and $\bar{\alpha}_{\text{Si}}$ as a function of the T_{surface} for $n_{\text{C}}^{\text{in}}/n_{\text{SiO}_2}^{\text{in}} = 1$, 2, and 4. For $n_{\text{C}}^{\text{in}}/n_{\text{SiO}_2}^{\text{in}}$, $\bar{\alpha}_{\text{Si}} < 1$, confirming the presence of amorphous SiO_2 for every

SURFACE TEMPERATURE

A heat transfer model was formulated for calculating the surface temperature of reactants exposed to concentrated radiation. The model domain is shown schematically in Figure C. The model couples radiation exchanged within the crucible, quartz tube, and reactant surfaces, and conduction across the layer of reactants and crucible. The boundary conditions were the measured incident solar radiative flux and the measured temperature of the backside of the crucible as the reaction neared completion. Based on comparable experiments,[19] T_{surface} was assumed constant for constant C. A two-band approximation was used to account for the transparent and opaque wavelength intervals of quartz, 0–λ_{c} and λ_{c}–∞, respectively, where $\lambda_{\text{c}} = 3.5$ μm. The radiative exchange for semi-transparent surfaces over the 0–λ_{c} bandwidth is given by Equation A.

The radiative exchange for opaque surfaces over the bandwidth from λ_{c}–∞ is given by Equation B, where q represents the net heat flux for a given surface over the first bandwidth, R and A denote the slab reflectance and absorptance, respectively, F represents the configuration factors between surfaces, H_o is the external contribution to the irradiation, E_{b} is Planck's total blackbody emissive power, f is the of the fractional function for a given surface temperature over 0–λ_{c}. Slab optical properties for the quartz tube were calculated using temperature-dependent absorption coefficients[20] and the index of refraction[21] with the Fresnel law. Convective heat exchange inside the reactor was neglected due to the evacuated chamber. Assuming 1-D steady-state conduction, the net heat flux through the crucible was calculated as Equation C, where k denotes thermal conductivity measured by the manufacturer, T_1 (= T_{surface}) and $\bar{T}_{\text{c}}$ represent the temperatures at the surface and backside of the crucible, respectively, and d represents the thickness of the crucible. The net heat flux to the quartz tube is given as Equation D, where h denotes the convective heat transfer coefficient calculated from a Nusselt correlation for vertical tubes at low Reynolds numbers,[22] T_2 and T_{amb} represent the surface temperature of the quartz tube and ambient temperature, respectively, and σ is the Stefan–Boltzmann constant. The temperature dependencies of all properties were accounted for by using an iterative scheme to solve the system of equations where the initial temperatures were guessed and updated until temperature convergences of less than 0.1 K were achieved. The total blackbody emissive power was linearized with a Taylor series expansion around the initial temperature guess and updated iteratively as Equation E, where T_g is the initial guess updated until convergence. The uncertainties for the surface temperatures due to error propagation of the inputs were estimated by a Monte Carlo analysis where the input parameters were perturbed according the manufacturer and published uncertainties.

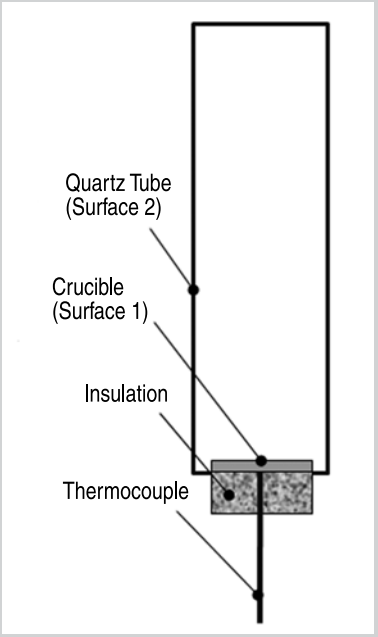

Figure C. Schematic of the vacuum reactor for the modeling radiative exchange between surfaces.

EQUATIONS

$$\frac{q_{\text{i}}^{(1)}}{1-R_{\text{i}}} - \sum_{\text{j}=1}^{\text{N}} \left(\frac{R_{\text{j}}}{1-R_{\text{j}}} \right) F_{\text{i-j}} q_{\text{j}}^{(1)} + H_{\text{oi}}^{(1)} = \frac{A_{\text{i}}}{1-R_{\text{i}}} E_{\text{b,i}} f\left(T_{\text{i}}\lambda_{\text{c}}\right) - \sum_{\text{j}=1}^{\text{N}} \left(\frac{A_{\text{j}}}{1-R_{\text{j}}} \right) F_{\text{i-j}} E_{\text{b,j}} f\left(T_{\text{i}}\lambda_{\text{c}}\right) \quad \text{(A)}$$

$$\frac{q_{\text{i}}^{(2)}}{\varepsilon_{\text{i}}} - \sum_{\text{j}=1}^{\text{N}} \left(\frac{1}{\varepsilon_{\text{j}}} - 1 \right) F_{\text{i-j}} q_{\text{j}}^{(2)} = \left(1 - f(T_{\text{i}}\lambda_{\text{c}})\right) E_{\text{b,i}} - \sum_{\text{j}=1}^{\text{N}} F_{\text{i-j}} \left(1 - f(T_{\text{j}}\lambda_{\text{c}})\right) E_{\text{b,i}} \quad \text{(B)}$$

$$q_1^{(1)} + q_1^{(2)} = -k \frac{T_1 - \bar{T}_{\text{c}}}{d} \quad \text{(C)}$$

$$q_2^{(1)} + q_2^{(2)} = V_2 \left(\frac{q_2^{(1)} - A_2 f(T_2\lambda_{\text{c}}) E_{\text{b,2}}}{1-R_2} \right) - h\left(T_2 - T_{\text{amb}}\right) - A_2 f(T_2\lambda_{\text{c}}) E_{\text{b,2}} - \varepsilon_2 \left(1 - f(T_2\lambda_{\text{c}})\right) E_{\text{b,2}} + \varepsilon_{\text{amb}} \sigma T_{\text{amb}}^4 \quad \text{(D)}$$

$$E_{\text{b,i}} = \sigma T_{\text{g,i}}^4 + 4\sigma T_{\text{g,i}}^3 \left(T_{\text{i}} - T_{\text{g,i}}\right) \quad \text{(E)}$$

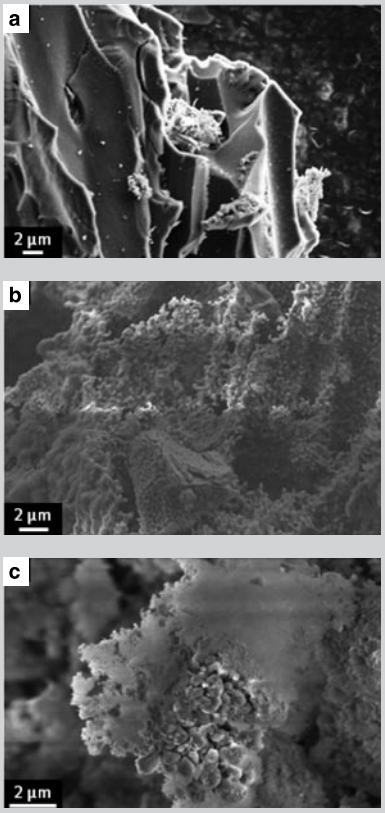

Figure 7. SEM pictures of (a) reactants, (b) solid products that remained in the crucible, and (c) solid products deposited in the quartz tube.

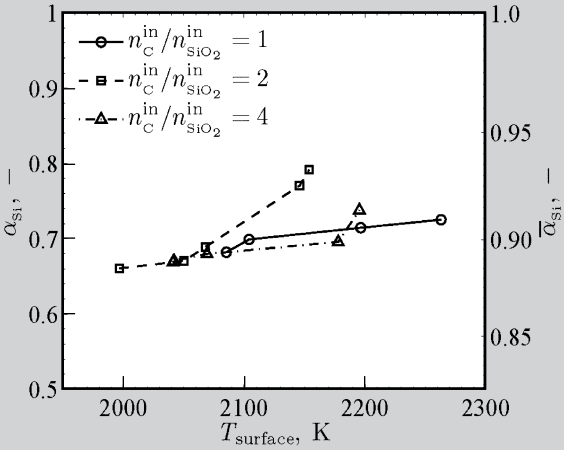

Figure 8. Mass and molar silicon purity from ICP of the samples scraped from the dome of the reactor as a function of the surface temperature for C:SiO_2 molar ratio of 1(circles), 2 (squares), and 4 (triangles).

experiment where α_{Si} increased with increasing $T_{surface}$. α_{Si} and $\bar{\alpha}_{Si}$ ranged from 0.807–0.890 and 0.725–0.854, respectively, indicative of Si(g) and SiO(g) distilling off from the crucible.

Reaction Scheme

The carbothermal reduction of SiO_2 to Si can be represented by four key reactions that included SiO and SiC as intermediaries[24] (given as Equations 5–8).

These series of reactions are consistent with the thermodynamic equilibrium predictions and the findings from experimentation in the solar reactor where SiC was always detected as a solid product in the crucible but never in the condensed products collected from the quartz tube. The low r_m for $n_C^{in}/n_{SiO_2}^{in} = 1$ is attributed to C being used up in Reactions 4–5 and SiO(g) leaving the system. Larger r_m for $n_C^{in}/n_{SiO_2}^{in} = 2$ is attributed to both Si and SiO leaving in the gaseous form. When $n_C^{in}/n_{SiO_2}^{in} = 4$ in the presence of excess charcoal, higher conversions from SiO_2 to Si were estimated from the temporal CO measurements, consistent with the entire reaction scheme.

CONCLUSIONS

Reducing the total pressure in the carbothermal reduction of SiO_2 causes a shift in equilibrium that forecasts the formation of Si(g) at lower temperatures. Experimentation was performed in a solar reactor at ~3×10^{-3} bar with reactants directly exposed to simulated high-flux solar radiation. A suite of experiments was performed with carbon to silica molar ratios of 1–4 and surface temperatures in the range 1,997–2,263 K. As expected, the highest conversions of carbon to CO were obtained with excess silica and all conversions for all molar ratios increased with increasing temperatures. Solid product that remained in the crucible, analyzed by XRD, contained SiC and, in some cases, Si. Solid product that deposited on the quartz tube analyzed by ICP revealed that in addition to Si other Si-O compounds were present and thought to have amorphous structures because XRD analysis only detected Si in all but three cases where SiO_2 was detected. However, no carbides were found in those samples. These results were found to be consistent with a reaction scheme with SiO and SiC as intermediaries.

ACKNOWLEDGEMENTS

We thank A. Frei and H. Yoon for the chemical analysis, and L. Schlumpf, Y. Baeuerle, D. Meyer, P. Schaller, and D. Wuillemin for the operation of the PSI's High-Flux Solar Simulator.

References

1. A. Luque and S. Hegedus, *Handbook of Photovoltaic Science and Engineering* (Chichester, U.K.: John Wiley & Sons LTD, 2003).
2. W. Zulehner et al., "Silicon," *Ullmann's Encyclopedia of Industrial Chemistry* (Weinheim, Germany: Wiley-VCH Verlag GmbH & Co. KGaA, 2005).
3. D. Sarti and R. Einhaus, *Sol. Energ. Mat. Sol. C.*, 72 (2002), pp. 27–40.
4. P. Woditsch and W. Kock, *Sol. Energ. Mat. Sol. C.*, 72 (2002), pp. 11–26.
5. K. Yasuda et al., *Electrochim. Acta,* 53 (2007), pp. 106–110.
6. G. Flamant et al., *Sol. Energ. Mat. Sol. C.*, 90 (2006), pp. 2099–2106.
7. J.P. Murray, A. Steinfeld, and E.A. Fletcher, *Energy,* 20 (1995), pp. 695–704.
8. J.P. Murray, G. Flamant, and C.J. Roos, *Sol. Energy*, 80 (2006), pp. 1349–1354.
9. A.W. Weimer et al., *J. Mater. Sci.,* 31 (1996), pp. 6005–6013.
10. A. Steinfeld and E.A. Fletcher, *Energy,* 16 (1991), pp. 1011–1019.
11. R. Adinberg and M. Epstein, *Energy*, 29 (2004), pp. 757–769.
12. T. Osinga, G. Olalde, and A. Steinfeld, *Ind. Eng. Chem. Red.*, 43 (2004), pp. 7981–7988.
13. M. Epstein et al., *J. Sol. Energ-T ASME,* 130 (2008), pp. 14505-1–4.
14. M.E. Galvez et al., *Int. J. Hydrogen Energ.*, 33 (2008), pp. 2880–2890.
15. M. Halmann, A. Frei, and A. Steinfeld, *Energy*, 32 (2007), pp. 2420–2427.
16. M. Halmann, A. Frei, and A. Steinfeld, "Aluminum Carbothermic Production with Excess Alumina and Reduced Pressure," *Proc. ECOS 2010—23rd International Conference on Efficiency, Costs, Optimization, Simulation and Environmental Impact of Energy Systems* (Lausanne, Switzerland: EPFL, 2010).
17. A. Roine, Outokumpu, *HSC Chemistry for Windows 5.0* (Pori, Finland: Outokumpu Research, 1997).
18. J. Petrasch et al., *J. Sol. Energ-T ASME,* 129 (2007), pp. 405–411.
19. S.M. Schnurre, J. Groebner, and R. Schmid-Fetzer, *J. Non-Chryst. Solids*, 336 (2004), pp. 1–25.
20. D.H. Filsinger and D.B. Bourrie, *J. Am. Ceram. Soc.*, 73 (1990), pp. 1726–1732.
21. L.O. Schunk, W. Lipinsky, and A. Steinfeld, *AIChE J.,* 55 (2009), pp. 1659–1666.
22. E.C. Beder, C.D. Bass, and W.L. Shackleford, *Appl. Optics,* 10 (1971), pp. 2263–2268.
23. W.S. Rodney and R.J. Spindler, *J. Opt. Soc. Am.,*(1954), pp. 677–679.
24. L.C. Burmeister, *Convective Heat Transfer,* 2nd Edition (New York: John Wiley & Sons Inc, 1993).

Peter G. Loutzenhiser, lecturer and research associate, Ozan Tuerk, master student, and Aldo Steinfeld, professor, are with the Department of Mechanical and Process Engineering, ETH Zurich, 8092 Zurich, Switzerland. Dr. Steinfeld is also with Solar Technology Laboratory, Paul Scherrer Institute, 5232 Villigen, Switzerland and can be reached at aldo.steinfeld @ethz.ch.